# Correlative Signal Processing in Wireless SAW Sensor Applications to Provide Multiple-Access Capability

Gerald Ostermayer, *Associate Member, IEEE*

***Abstract*—We present a new method of evaluating the information of interest in the output response of surface acoustic wave (SAW) sensors. A well-known spread-spectrum technique is used to get the sensor information from an individually addressed SAW sensor. On–off keying-coded SAW sensors are picked out of a number of sensors by correlating the sensor response signal with a replica of the known response signal of a particular sensor. The influence of a measurement quantity (e.g., temperature, pressure, current, voltage, . . .) to a SAW sensor can be observed as a scaling of time and shape of the sensor response signal. This scaling factor is evaluated by use of correlative signal processing techniques. A main advantage of this method is the capability of multiple access, i.e., to distinguish different sensors in the range of a single interrogation system. Since this technique makes it possible to deal with sensor response signals overlapping in the time domain, sensors can remain short and, therefore, cheap. The principle of operation, limits of the method, and experimental results for temperature measurements are also presented.**

***Index Terms*—Correlative signal processing, multiple access, SAW, sensors.**

## I. Introduction

TOGETHER with the extending application of electronically controlled systems, sensor technology is growing rapidly. In many remote-sensing applications, a reliable wire connection between the sensor and measurement cannot be installed. In addition, the automation of many processes requires secure identification of tools and work pieces. Therefore, for measuring the air pressure in tires of cars, for monitoring the temperature within closed chambers, for person identification, etc., systems with wirelessly interrogable sensors have been developed. Most of these systems contain active semiconductor circuits, a sensor circuit, and a transceiver unit. Often they are powered by small batteries. The remote systems transmit their data that contain the sensor information.

In some applications, remote sensor systems are affected by strong thermal, mechanical, or electromagnetic load in a way that batteries, semiconductors, and active elements are likely to be damaged. Further, if the sensor is mechanically inaccessible, the life time of a battery supplied sensor gets critical. In all these cases, SAW sensors can be used advantageously. A problem arises in case of multiple access, i.e., if more than a single sensor is in the range of an interrogation system. Commonly used measurement evaluation techniques [1], [2] fail if the sensors are not time orthogonal. In Section II, we present a short description of surface acoustic wave (SAW) sensors. Further, we discuss the multiple-access problem. In Section III, the sensor property of a SAW device is described. In Section IV, we introduce a novel method of getting the sensor information, which is a solution for the multiple-access problem. The limits of this technique are also discussed. Section V shows the implementation of the concept for practical use. In Section VI, we present measurement results. Conclusions are then presented in Section VII.

Manuscript received October 18, 2000; revised January 15, 2001.

The author is with PSE MCS RA 2, Siemens AG Österreich, A-1101 Vienna, Austria.

Publisher Item Identifier S 0018-9480(01)02907-6.

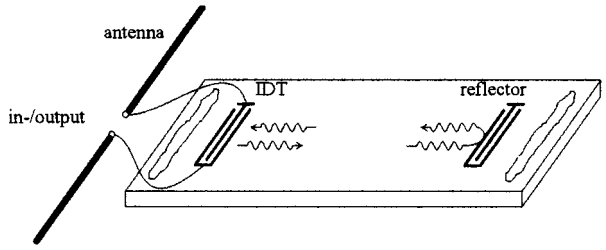


Fig. 1. SAW delay line sensor.

## II. SAW Sensors and Multiple Access

Some years ago, the applicability of passive SAW devices for remote sensing was found [2]–[5]. These sensors can be built with a SAW delay-line element connected to an antenna. Fig. 1 depicts a passive SAW delay line [6] that can be interrogated wirelessly. The interdigital transducer (IDT) [7] is the element that transforms an electrical signal to a SAW and vice versa. Connecting this IDT to an antenna provides the possibility of a wireless interrogation of the device. The IDT transforms an electrical input signal to a SAW propagating along the substrate surface. At the reflecting structure, the SAW is (partly) reflected and it propagates back to the IDT where it is transformed to an electrical output signal. The IDT behaves like a reciprocal and linear time invariant (LTI) system with an electrical and acoustic gate and can be described with its electroacoustic impulse response $h_{ea}(t)$. For practical signal amplitudes (several 100 mV), the whole device can be considered as an LTI system with an electrical impulse response

$$\begin{aligned} h(t) &= h_{ea}(t) \cdot \alpha_a * r_a(t) * h_{ea}(-t) \cdot \alpha_a * \delta(t - 2T_a) \\ &= \alpha_a^2 \cdot \mathrm{ACF}_{h_{ea}}(t - 2T_a) * r_a(t). \end{aligned} \tag{1}$$

In (1), $L$ is the distance between the IDT and reflector, $a_a$ is the loss of the SAW amplitude along the length $L$, $r_a(t)$ is

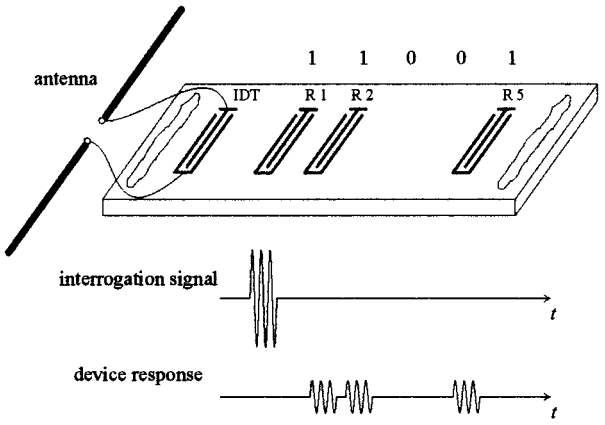


Fig. 2. OOK-coded SAW sensor.

the reflection coefficient of the reflector, $T_a = L/v$ is the time delay of the SAW along the distance $L$ ($v$ is the sound speed), and ACF is the autocorrelation function. Interrogation of such a device with a short RF burst results in an RF burst with smaller amplitude and time delay $2T_a$ as the response. It has to be stated that this model is quite simple and does not consider second-order effects such as dispersion on the acoustic delay line and the reflector or reflections between the IDT and reflector. However, it describes the principle way of how such an element works.

This simple sensor type has the disadvantage that the required substrate length increases linearly with the number of sensors that have to be distinguished. This is because these elements are distinguished by the distance between the IDT and reflector. This results in enormous costs since the production costs of a sensor increase approximately with the third power of its length. A possible solution is the use of more than one reflective structure at well-defined places. Fig. 2 shows such a coded identification (ID)-tag-type sensor with the interrogation signal and sensor response signal. Three bits are set to "1" and two more bits are set to "0" by leaving out the reflectors. The sensor has its individual code [1 1 0 0 1] with code-type on–off keying (OOK).

A problem arises if there are some ID-tag-type SAW sensors in the range of a single interrogation system. The intention of using coded sensors is to have the ability to distinguish many short (and, therefore, cheap) sensors. The price to pay is that the sensor responses are no longer orthogonal. The superposition of all the sensor response signals results in the problem of evaluating the information about the measurement quantity of each sensor. How to deal with this problem is described below.

## III. Sensor Effect

As explained in Section I, the sensor behaves like an LTI system. The output signal $y(t)$ of an LTI system can be described by a convolution of the input signal $x(t)$ with the impulse response $h(t)$

$$\begin{aligned} y(t) &= x(t) * h(t) \\ &= \int_{-\infty}^{\infty} x(\tau) \cdot h(t-\tau)\, d\tau \\ &= \int_{-\infty}^{\infty} x(t-\tau) \cdot h(\tau)\, d\tau. \end{aligned} \tag{2}$$

In case of a sensor, the time-dependent impulse response is additionally dependent on the measurement quantity and often dependent on the temperature. In general, this temperature dependence (exception: temperature sensors) disturbs the measurement. Using differential measurements, this influence can be reduced. In the following, we assume the impulse response to be dependent only on time and the measurement quantity. The sensor output signal $y$ also depends on time $t$ and the measurement quantity $M$

$$y(t, M) = x(t) * h(t, M). \tag{3}$$

Let us consider the impulse response $h(t, M)$. A SAW sensor can be influenced by a measurement quantity in different ways. If the substrate is stretched or compressed (e.g., by a mechanical or temperature influence), it changes its mechanical dimensions. This results in a change of the acoustic length. Additionally, the sound velocity determined by substrate properties change. Thus, measurement quantities can affect two sensor parameters: the mechanical dimensions and/or the velocity of the propagating SAW. In most cases, it is a combination of both. The effect on the interesting impulse response with length $T$ is the same in both cases: it is stretched or compressed by the length $\Delta T$. The relative change of the time duration $\varepsilon$ is given by $\varepsilon = \Delta T/T$. This leads to

$$T + \Delta T = T + \varepsilon \cdot T = s \cdot T \tag{4}$$

with $s = 1 + \varepsilon$ as the so-called scaling factor. Additionally, the impulse response suffers a time delay $\tau$ due to electromagnetic and acoustic delay. The time variable $t$ is transformed to

$$t \mapsto \frac{t - \tau}{s}. \tag{5}$$

Scaling of the time axis and the time delay is given by the factors $s_h$ and $\tau_h$. Equation (3) can now be rewritten to

$$y(t, M) = y\Big(t, s_h(M), \tau_h(M)\Big) = x(t) * h\left(\frac{t - \tau_h(M)}{s_h(M)}\right). \tag{6}$$

It is concluded that the measurement quantity affects the sensor in a way that its impulse response is scaled and delayed in time. Both the time scaling factor and time delay contain the whole sensor information. Note that there are also sensors imaginable where the two previous statements are violated. In this paper, we are considering sensor configurations where these statements hold. For the sensing purposes at hand, we focus on the time scaling factor. If the connection between scaling factor and measurement quantity is well known and the impulse response $h((t - t_h)/s_h, M)$ is accessible to measurements, then the evaluation of the sensor information is reduced to the evaluation of the scaling factor $s_h$ of the impulse response.

If the impulse response is not accessible, then the sensor response signal $y$ has to be taken to evaluate the sensor information. The signal $y$ is affected in its time behavior as well. In general, this change is not only dependent on the measurement quantity, but additionally dependent on the interrogation signal

$x$. This interrogation signal is a short RF burst. The sensor answers with a signal resulting from the convolution of the interrogation signal with the sensor impulse response. This signal is described as burst response. The shorter the burst, the smaller the difference between impulse response and burst response. The question arises as to how the time scaling of the impulse response affects the burst response. From Fig. 2, one can see that three parameters of the impulse, as well as the burst response, are affected by the measurement quantity: the time shift of the bursts to each other, the time duration of the bursts, and the waveform of the bursts. All these three parameters of the impulse response are time scaled by the factor $s_h$.

Let us now take a closer look at the burst response. The relative distance between two reflected bursts of the burst response is scaled by $s_h$ as well. Now we focus on a single reflected burst. The time duration, as well as the waveform of the reflected burst, is affected by the measurement quantity in a slightly different way. The influence of the reflectors are neglected since they are much shorter than the IDT. This assumption leads to the simplification $r_a(t) = \delta(t)$. Remembering (1) and (2), setting $a_a = 1$, and neglecting the time delay $2T_a$ (does not affect the interesting parameters), we get for the normalized reflected burst

$$y_B(t) = x(t) * h_{ea}(t) * h_{ea}(-t) = x(t) * \mathrm{ACF}_{h_{ea}}(t). \quad (7)$$

With this result, the time duration $T_B$ and the scaling factor $s_B$ of the reflected burst can be determined. For the time duration, we get

$$T_B = T_x + 2T_h \quad (8)$$

with $T_x$ and $T_h$ as the time duration of the interrogating burst $x(t)$ and the impulse response $h_{ea}(t)$ of the IDT. Scaling $h_{ea}(t)$ with the factor $s_h$ yields to a modified length $T_B' = s_B \cdot T_B$ of the reflected burst. The scaling factor $s_B$ can be evaluated to

$$s_B = \frac{T_x + s_h \cdot 2T_h}{T_x + 2T_h} = \frac{s_h + \dfrac{T_x}{2T_h}}{1 + \dfrac{T_x}{2T_h}}. \quad (9)$$

For $T_x/2T_h \ll 1$, the scaling factors of the reflected burst and of the impulse response are equal, i.e., $s_B = s_h$. This means that the interrogating burst has to be much shorter than the length of the IDT. With this assumption, (6) can be rewritten as

$$y(t, M) = yt\Big(t, s_h(M), \tau_h(M)\Big) = y\left(\frac{t - \tau_h(M)}{s_h(M)}\right). \quad (10)$$

This means that the burst response (with a sufficiently short interrogation burst) is affected by the measurement quantity in the same way as the impulse response, i.e., time scaling with factor $s_h$ and time shift with delay $\tau_h$. Consequently, we can use this burst response to evaluate the scaling factor $s_h$ and, therefore, to evaluate the sensor information.

## IV. System Concept

### A. Principles

In Section II, we described how to implement multiple access (several sensors in the range of a single interrogation signal). Using individually coded sensors provides the capability to distinguish sensors, as well as to evaluate their individual sensor information even if their burst responses are not time orthogonal to each other. All the sensors are interrogated with the same RF burst and each sensor answers with its individual burst response. At the receiver, a superposition of all these individually scaled burst responses appear. It is the task of the receiving part of the interrogation system is to evaluate the scaling factor of each sensor. A feasible approach is to use correlative signal processing. The idea is to correlate the sum of the differently scaled sensor responses with a replica of the burst response of that sensor which we want to pick out [8], [9]. This correlation is repeated with scaled (by a factor $s_R$) versions of the sensor burst response replica generated in the receiver. In case the factor $s_R$ matches best, the highest correlation peak appears. A mathematical tool providing this operation is the wavelet transform (WT). In [10], the WT $W_g f(s, \tau)$ for real signals is defined by

$$W_g f(s, \tau) = \frac{1}{\sqrt{|s|}} \int_{-\infty}^{\infty} f(t) \cdot g\left(\frac{t - \tau}{s}\right) dt. \quad (11)$$

Here, $W_g f(s, \tau)$ is the WT of the function $f(t)$ with respect to the so-called "mother wavelet" $g(t)$ with the scaling factor $s$ for the particular calculation. The first term is a normalization factor providing constant signal energy for variable $s$. The mother wavelet is the reference signal with $s = 1$ and $\tau = 0$—in the present case, the unscaled replica of the burst response of the selected sensor. Due to this special choice of the mother wavelet and the resulting close connection to the radar wide-band cross-ambiguity function [11], we call this special function the scaling ambiguity function (SAF). The SAF calculates the cross correlation function (CCF) between the received signal $f(t)$ (the sum of the burst responses of all sensors) and differently scaled versions of the mother wavelet $g(t)$ (the unaffected burst response of the interesting sensor) as a function of $s$ and $\tau$. The matching scaling factor $s_M$ and the matching time delay $\tau_M$ correspond to the highest correlation peak of the SAF. Fig. 3 illustrates the principle.

### B. System Limits

In the preceding section, we described how the sensor information can be received by estimating the scaling factor $s_h$ of the sensor burst response. In principle, this can be done by correlating the sensor burst response with differently scaled versions of the so-called reference signal. The reference signal is generated in the receiver and is a replica of the burst response of the nominal sensor defined by the scaling factor $s_h = 1$. The nominal sensor is the sensor affected by a well-defined measurement quantity, e.g., room temperature for a temperature sensor. The maximum of the CCF varies with the scaling factor $s_R$ of the replica. The highest maximum appears in case the scaling factor of the replica and scaling factor of the burst response are the same, i.e., $s_h = s_R$. This method works as long as the highest peak of the CCFs (= maximum of the SAF) appears if $s_h = s_R$ is valid. However, this is only true within certain limits of the scaling factor around $s = 1$. According to the impulse model [13], the acoustic output signal $y_a(t)$ of the IDT

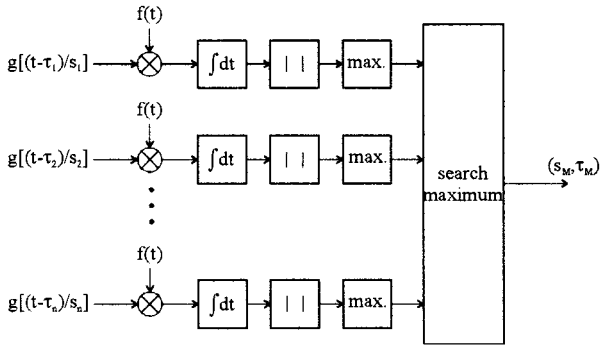


Fig. 3. Principle of searching the matching scaling factor $s_M$.

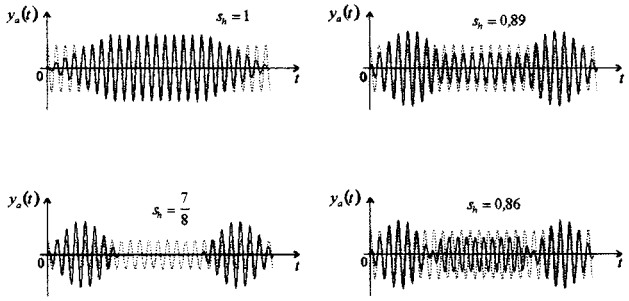


Fig. 4. Differently scaled acoustic output signal of an IDT (solid line) and a cosine wave with the corresponding frequency (dashed line).

can be written as the convolution of the electroacoustic impulse response $h_{ea}(t)$ and the electrical input signal $x(t)$

$$y_a(t) = x(t) * h_{ea}(t) = \int_{-\infty}^{\infty} x(\tau) h_{ea}(t-\tau)\, d\tau \qquad (12)$$

with

$$h_{ea}(t) = A_h \cdot \cos\left(2\pi \frac{f_0}{s_h} t\right) \cdot \Big[\sigma(t) - \sigma(t - s_h T_h)\Big] \qquad (13)$$

and

$$x(t) = A_x \cdot \cos(2\pi f_0 t) \cdot \Big[\sigma(t) - \sigma(t - T_x)\Big] \qquad (14)$$

where $\sigma$ denotes the step function. For the case $s_h \cdot T_h > T_x$, we get (15), shown at the bottom of this page, with $\varphi_1 = \pi f_0 \cdot (1-1/s_h)\cdot(T_x - s_h T_h)$, $\varphi_2 = -\pi f_0 \cdot (1-1/s_h)\cdot(T_x + s_h T_h)$, $\varphi_3 = \pi f_0 \cdot (1+1/s_h)\cdot(T_x - s_h T_h)$, and $\varphi_4 = -\pi f_0 \cdot (1+1/s_h)\cdot(T_x + s_h T_h)$.

Equation (15) shows that the acoustic output signal $y_a(t)$ of the IDT can be separated into three parts. Fig. 4 shows this signal for different scaling factors and a cosine wave with the corresponding frequency. The phase of the first and the third parts of the signal is not very sensitive to varying scaling factors. In contrast, the second (middle) part of the signal is extremely sensitive to varying scaling factors and, thus, determines the allowed range of the scaling factor. With increasing distance of $s_h$ from one (in both directions), the amplitude of the oscillation decreases down to zero. Going on with varying $s_h$ in the same direction, the amplitude of the oscillation increases, but the phase changes from zero up to $\pi$. From (15), we can find the scaling factor when the amplitude of the oscillation in the middle area equals zero. Within these limits, it is guaranteed that the maximum of the SAF appears in case $s_h = s_R$. These limits determine the scaling factor range (and, therefore, the measurement range) of such a system. For scaling factors around one,

$$y_a(t) = \begin{cases} A_x A_h \dfrac{\cos\left[\pi f_0\left(1+\frac{1}{s_h}\right)t\right]\cdot\sin\left[\pi f_0\left(1-\frac{1}{s_h}\right)t\right]}{2\pi f_0\left(1-\frac{1}{s_h}\right)} + A_x A_h \dfrac{\cos\left[\pi f_0\left(1-\frac{1}{s_h}\right)t\right]\cdot\sin\left[\pi f_0\left(1+\frac{1}{s_h}\right)t\right]}{2\pi f_0\left(1+\frac{1}{s_h}\right)}, \\ \qquad 0 \le t < T_x \\ A_x A_h \dfrac{\cos\left[2\pi\frac{f_0}{s_h}t + \pi f_0\left(1-\frac{1}{s_h}\right)T_x\right]\cdot\sin\left[\pi f_0\left(1-\frac{1}{s_h}\right)T_x\right]}{2\pi f_0\left(1-\frac{1}{s_h}\right)} \\ +A_x A_h \dfrac{\cos\left[2\pi\frac{f_0}{s_h}t - \pi f_0\left(1+\frac{1}{s_h}\right)T_x\right]\cdot\sin\left[\pi f_0\left(1+\frac{1}{s_h}\right)T_x\right]}{2\pi f_0\left(1+\frac{1}{s_h}\right)}, \qquad T_x \le t < s_h T_h \\ -A_x A_h \dfrac{\cos\left[\pi f_0\left(1+\frac{1}{s_h}\right)t + \varphi_1\right]\cdot\sin\left[\pi f_0\left(1-\frac{1}{s_h}\right)t + \varphi_2\right]}{2\pi f_0\left(1-\frac{1}{s_h}\right)} \\ -A_x A_h \dfrac{\cos\left[\pi f_0\left(1-\frac{1}{s_h}\right)t + \varphi_3\right]\cdot\sin\left[\pi f_0\left(1+\frac{1}{s_h}\right)t + \varphi_4\right]}{2\pi f_0\left(1+\frac{1}{s_h}\right)}, \qquad s_h T_h \le t < s_h T_h + T_x \end{cases} \qquad (15)$$

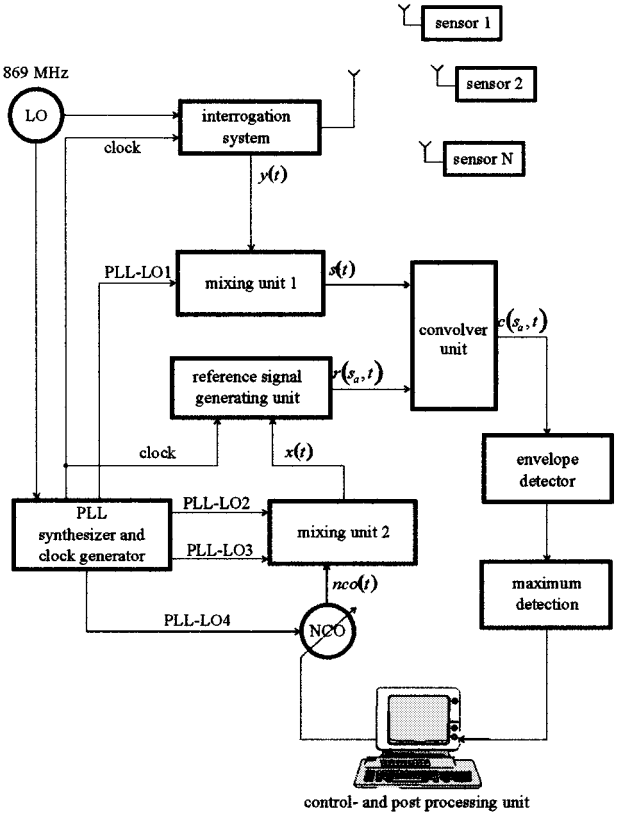


Fig. 5. Implemented system.

the second part of the middle area of (15) is negligible compared to the first part. We get

$$\cos\left[2\pi\frac{f_0}{s_h}t+\pi f_0\left(1-\frac{1}{s_h}\right)T_x\right]\cdot\sin\left[\pi f_0\left(1-\frac{1}{s_h}\right)T_x\right]=0,\quad s_hT_h>T_x. \tag{16}$$

Finally, we get for the limits of $s_h$

$$\frac{1}{1+\dfrac{1}{f_0\cdot T_x}}\le s_h\le\frac{1}{1-\dfrac{1}{f_0\cdot T_x}},\qquad s_hT_h>T_x. \tag{17}$$

As an example, we have $T_h=300$ ns, $T_x=20$ ns, and $f_0=869$ MHz. Therefore, we get a permissible scaling range of $0.946\le s_h\le 1.061$. For a temperature sensor with $LiNbO_3$ (temperature coefficient TCD $\approx$ 90 ppm/K), this corresponds to a temperature range of about 1270 K. From (7) and (11), we know that the sensor burst response is given by $y(t)=y_a(t)*h_{ea}(t)$. The described change in phase can be observed for the burst response as well. However, it is much more complicated to find the limits analytically. Simulations show that these limits are quite similar to those of $y_a(t)$, but a little bit more relaxed. Thus, using the limits of (17) guarantees that one is on the safe side.

## V. Implementation

Fig. 5 shows the whole system. The sensor interrogation system generates short RF bursts (20 ns–10 $\mu$s) at a center frequency $f_0=869$ MHz. Time gating separates the interrogation signal and the sensor burst responses, which are input for the convolver module. The second convolver input is the reference signal. The OOK code of the reference signal can be chosen arbitrarily with the control and post-processing unit. A code length up to 32 b is possible. Fig. 6 shows three examples of differently coded reference signals. The scaling of the reference signal is achieved by a numerically controlled oscillator (NCO), which provides a very high resolution of the center frequency (some millihertz). The OOK code of the reference signal is achieved by time gating of the continuous wave (CW) output of the NCO. Since this time gating is derived from the NCO frequency, the number of periods of a burst is constant. This provides the time scaling capability of the reference signal. An example is shown in Fig. 7.

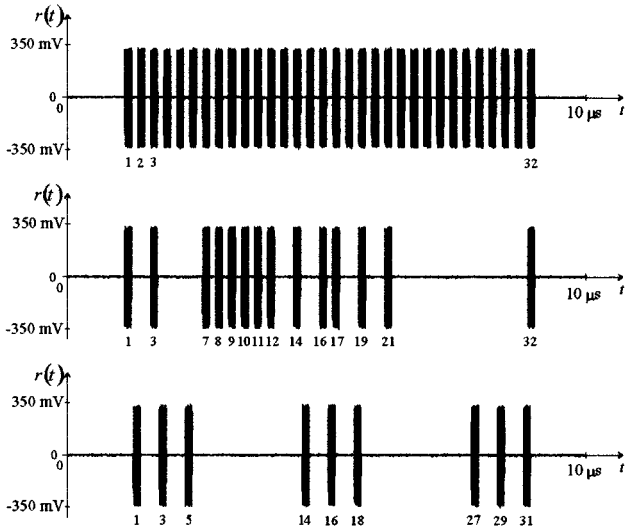


Fig. 6. Three differently coded reference signals.

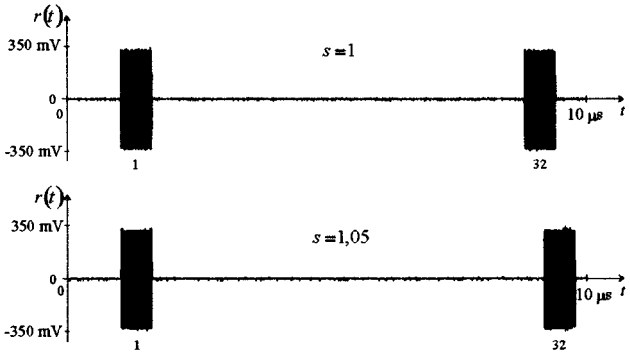


Fig. 7. Two differently scaled versions of a reference signal.

The convolver unit is shown in Fig. 8. Beside the convolver itself, it consists of passband filters, amplifiers, and matching networks. The convolver unit provides the possibility of real-time correlation of the burst responses with the differently scaled reference signals. The main parameters of the used convolver are its bandwidth $B=160$ MHz and integration duration $T_i=16\,\mu$s. Thus, it is possible to perform real-time convolutions of signals with a time bandwidth product of $T_i\cdot B=2560$. The CCF of the burst responses of the interrogated sensors and reference signal is available at the output of the convolver module. Fig. 9 shows an example with the same (but not symmetrical)

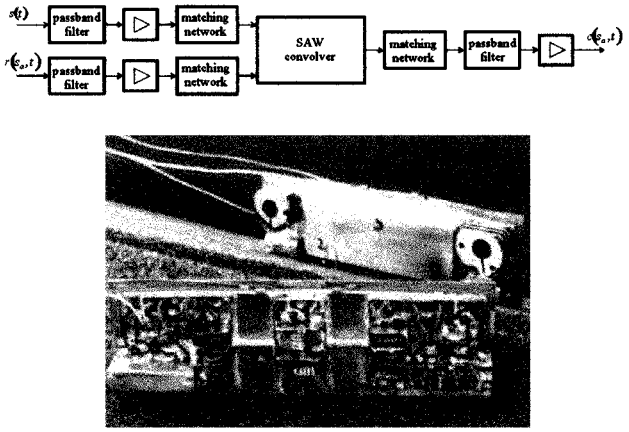


Fig. 8. Convolver unit.

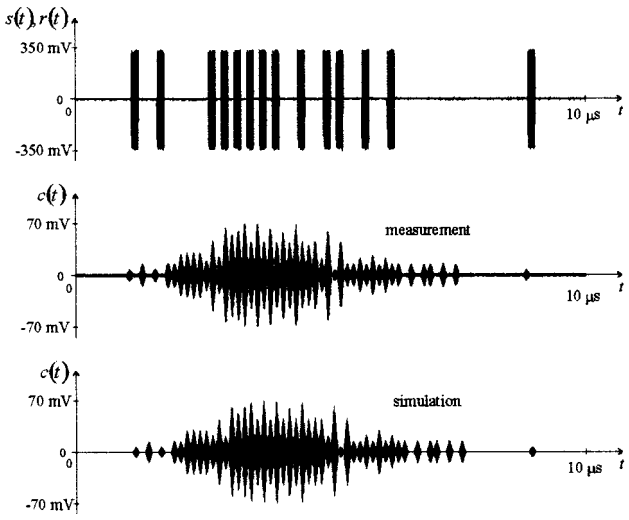


Fig. 9. Convolver input signals $s(t)$ and $r(t)$, measured and simulated convolver output signal $c(t)$.

signal at both convolver inputs. It can be seen that there is a perfect match between measurement and simulation.

The maximum detector determines the maximum of each CCF. Fixed phase relations of all used signals is guaranteed since all signals are derived from a single master clock at 869 MHz. The scaling range at 869 MHz is given by $1 \leq s_{\mathrm{SENSOR}} \leq 1019$. For an $LiNbO_3$ temperature sensor, this corresponds to a measurement range of about 210 K.

## VI. Measurements

### A. Sensors

For our measurements, there were four differently coded OOK sensors available, which are not time orthogonal. Fig. 10 shows the burst responses of the sensors $A$–$D$. The different averaged amplitudes of the different sensors are caused by different insertion losses. The varying amplitudes of different bursts of the same sensor are caused by different reflection coefficients of the reflective structures on the substrate surface. Fig. 11 shows the burst response of sensor $A$ at different

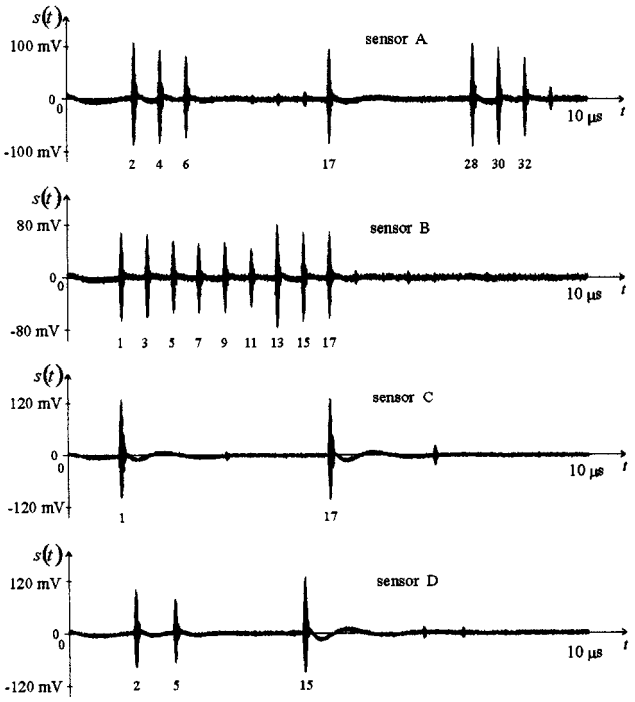


Fig. 10. Burst responses of the sensors $A$–$D$.

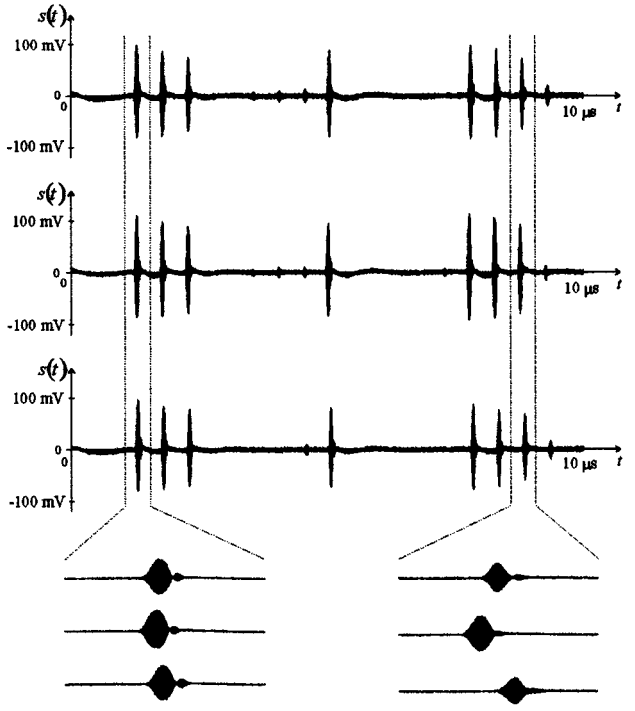


Fig. 11. Burst response of sensor $A$ at different temperatures.

temperatures. The upper curve is a measurement at room temperature, the middle curve shows the behavior of a cooled sensor, and the lower curve points out the behavior of a heated sensor. The delay of the reflected bursts can be seen very clearly.


Fig. 12. CCF of sensor $A$'s burst response with differently scaled reference signals ($s_1 = 1.001174$ and $s_2 = 1.0011167$).

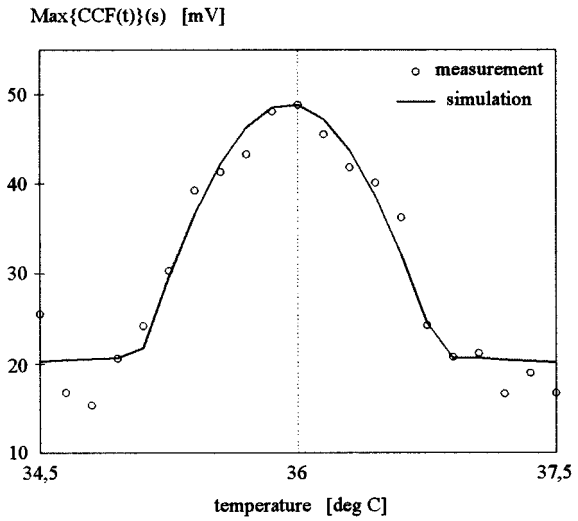


Fig. 13. Behavior of the maxima of the CCF dependent on temperature for sensor $A$ at 36 °C.

### B. Temperature Measurements

The connection between temperature and scaling factor of the burst response is given by

$$\vartheta = \vartheta_0 + \frac{s_{\mathrm{SENSOR}} - 1}{\mathrm{TCD}} \tag{18}$$

with $\vartheta_0$ as the temperature of the unscaled sensor (room temperature $\vartheta_0 = 23\,^{\circ}\mathrm{C}$). For the used $LiNbO_3$ sensors, the temperature coefficient is given by $\mathrm{TCD} = 90$ ppm/K $= 9 \cdot 10^{-5}$/K.

Sensor $A$ was warmed up to 36 °C. Fig. 12 shows the CCF (= convolver output signals) of the burst response and two differently scaled ($s_1 = 1.001174$ and $s_2 = 1.0011167$) reference signals. The difference between $s_1$ and $s_2$ is very small, $s_1 - s_2 = 0.0000573$. This difference corresponds to a temperature difference of 0.64 K. One can see that, even for this small temperature difference, a clear difference in the maximum value of each of these signals can be observed. Fig. 13 shows the behavior of the maxima of the CCFs dependent on temperature. These temperature values correspond to certain scaling factors of the reference signal. The scaling factor at the highest maximum of CCF can be evaluated to $s_{\mathrm{SENSOR}} = 1.001174$. Using (18), we get a temperature $\vartheta = 36.05$ °C, which is very close to the value of 36 °C given by the reference measurement using a thermo element. The resolution of the measurement with the SAW sensor is given by the resolution of the NCO. In our case, the NCO resolution is below 1 Hz, which leads to a temperature resolution of some millikelvin.

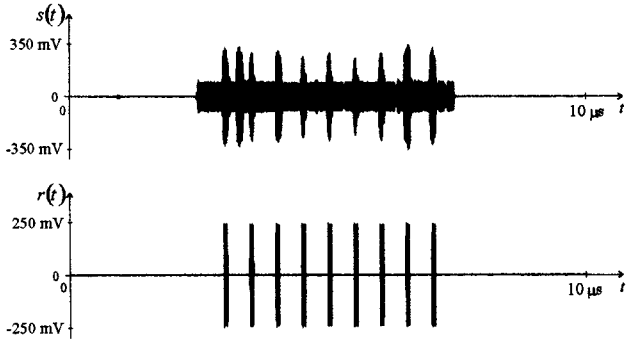


Fig. 14. Sum of the burst responses of three sensors at different temperatures (sensor $B$ at 48 °C, sensor $C$ at 40 °C and sensor $D$ at 28 °C) and the reference signal for sensor $B$.

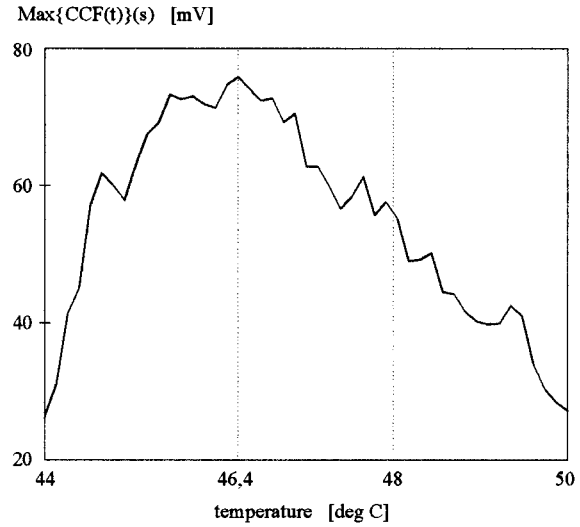


Fig. 15. Temperature measurement in case of multiple access; sensor $B$ is interfered by sensors $C$ and $D$.

The next measurement was performed with three different sensors ($B$, $C$, and $D$) at the temperatures $\vartheta_B = 48\,^{\circ}\mathrm{C}$, $\vartheta_C = 40\,^{\circ}\mathrm{C}$, and $\vartheta_D = 28\,^{\circ}\mathrm{C}$ to demonstrate the multiple-access capability. We tried to evaluate the temperature of sensor $B$, which was interfered by sensors $C$ and $D$ at the bits 1, 5, 15, and 17. In Fig. 14, one can see the sum of the burst responses of the three sensors. The bursts 1, 5, 15, and 17 are wider than the others since they result from an overlapping of differently scaled burst responses. Additionally, the reference signal can be seen. Fig. 15 shows that the measurement result is given by 46.4 °C. Since the correct value is 48 °C, the interference caused by sensors $C$ and $D$ results in a systematic measurement error of 1.6 °C. The systematic error is caused by the lack of orthogonality. Note that any orthogonality of the selected OOK codes would be affected by the sensor scaling factor.

## VII. Conclusions

We presented a new method to get the information of a passive SAW sensor. In case of a multiple-access situation, this technique provides the capability to distinguish the sensors even if

their burst responses are not time orthogonal. Without the prerequisite of time orthogonal burst responses, the SAW sensors can remain short even if many sensors have to be distinguished. Short sensors can be manufactured economically since the costs of such a sensor approximately increase with the third power of its length.

Measurements on a prototype system show that this method provides excellent accuracy in case of a single sensor. In the multiple-access scenario, the accuracy is traded off against substrate length.

## ACKNOWLEDGMENT

The author thanks Prof. Dr. F. Seifert (retired), Applied Electronics Laboratory, University of Technology, Vienna, Austria, and Dr. A. Pohl, Siemens AG, Vienna, Austria, for continuous scientific advice and stimulating discussions. The author gratefully acknowledges Dr. L. Reindl , Institute of Electrical Information Technology, Technical University of Clausthal, Clausthal, Germany, for supporting this paper with excellent SAW devices and helpful discussions.

## REFERENCES

[1] A. Pohl, G. Ostermayer, and F. Seifert, "Wireless measurement of tire pressure using passive SAW sensors," in *Proc. SENSOR'97*, pp. 89–94.

[2] F. Seifert, W. E. Bulst, and C. Ruppel, "Mechanical sensors based on surface acoustic waves," *Sens. Actuators A, Phys.*, vol. 44, pp. 231–239, 1994.

[3] L. Reindl, F. Müller, C. Ruppel, W. E. Bulst, and F. Seifert, "Passive surface wave sensors which can be wirelessly interrogated," Int. Patent WO 93/13 495, 1992.

[4] P. A. Nysen, H. Skeie, and D. Armstrong, "System for interrogating a passive transponder carrying phase-encoded information," U.S. Patent 4725841, 4 625 207, 4 625 208, 1983–1986.

[5] W. Buff, "SAW sensors," *Sens. Actuators A, Phys.*, vol. 42, pp. 117–121, 1992.

[6] A. Pohl, F. Seifert, L. Reindl, G. Scholl, T. Ostertag, and W. Pietsch, "Radio signals for ID-tags and sensors in strong electromagnetic interference," in *Proc. IEEE Ultrason. Symp.*, 1994, pp. 195–198.

[7] R. M. White and F. W. Voltmer, "Direct piezoelectric coupling to surface elastic waves," *Appl. Phys. Lett.*, vol. 7, pp. 314–316, 1965.

[8] G. Ostermayer, A. Pohl, C. Hausleitner, L. Reindl, and F. Seifert, "CDMA for wireless SAW sensor applications," in *Proc. IEEE Int. Spread-Spectrum Tech. Applicat. Symp.*, 1996, pp. 795–799.

[9] A. Pohl, G. Ostermayer, C. Hausleitner, F. Seifert, and L. Reindl, "Wavelet transform with a SAW convolver for sensor application," in *Proc. IEEE Ultrason. Symp.*, 1995, pp. 143–146.

[10] L. G. Weiss, "Wavelets and wideband correlation processing," *IEEE Signal Processing Mag.*, vol. 11, pp. 11–32, Jan. 1994.

[11] P. M. Woodward, *Probability and Information Theory with Applications to Radar*. New York: Pergamon, 1953.

[12] X. Q. Bao, W. Burkhard, V. V. Varadan, and V. K. Varadan, "SAW temperature sensor and remote reading system," in *Proc. IEEE Ultrason. Symp.*, vol. 1, 1987, pp. 583–585.

[13] C. S. Hartmann, D. T. Bell, and R. C. Rosenfeld, "Impulse model design of acoustic surface wave filters," *IEEE Trans. Microwave Theory Tech.*, vol. MTT-21, pp. 162–175, Apr. 1973.

**Gerald Ostermayer** (S'98–A'99) received the Dipl.-Ing. and Dr.techn. degrees in communication engineering from the University of Technology (TU), Vienna, Austria, in 1992 and 1998, respectively. His doctoral research described the use of correlative signal processing in SAW sensor systems.

In 1992, he joined EBG, where he was a Design Engineer involved with high-voltage power transformers. In 1994, he joined the Applied Electronics Laboratory, Institut für Allgemeine Elektrotechnik und Elektronik, TU, where he was a Research and Teaching Assistant. In 1997, he joined PSE MCS RA2, Siemens AG Österreich, Vienna, Austria, during which time he has been involved in the field of third-generation (3G) mobile systems. His research interests are in the areas of network simulation and radio resource management (RRM) algorithms for 3G mobile systems.